RSC Advances

ROYAL SOCIETY OF CHEMISTRY

www.rsc.org/advances

Cite this: DOI: 10.1039/c0xx00000x

www.rsc.org/xxxxxx

ARTICLE TYPE

Mesoporous silica based reservoir for active protection of mild steel in aggressive chloride ion environment.

T.Siva[a],M.Sunder,[a]S.S. Sreejakumari,[b] S.Sathiyanarayanan[a]*

Received (in XXX, XXX) XthXXXXXXXXX 20XX, Accepted Xth XXXXXXXXX 20XX

DOI: 10.1039/b000000x

Spherical mesoporous silica (m-SiO_2) with well-ordered pores was synthesized by a modified stober method using CTAB micelles. The as-prepared silica was used as a reservoir to load the corrosion inhibitor. Steel samples coated with inhibitor loaded silica reservoir exhibited improved corrosion resistance than without silica reservoir in an aggressive chloride environment. Localised electrochemical impedance spectroscopy (LEIS) and scanning vibrating electrode technique (SVET) data suggest an inhibitor release triggered by the local corrosion phenomena leading to active protection of the metal.

Introduction

Performance improvement in corrosion control methods is the need of the day and eventually all process industries try incremental research to achieve the same. Organic coating, a major and proven domain of corrosion control has seen multi-directional advancements in the last decade. Avoiding the usage of carcinogenic / toxic ingredients in corrosion protective coatings is a yet another mile stone. Bio-mimitic coatings, intelligent/smart coatings, self healing coatings etc. use the borrowed knowledge from other frontier areas such as drug delivery, nature. Intelligent/smart coatings have built in mechanism to release the required corrosion inhibitor while ensuring the barrier effect of coating. This greatly reduces the degradation / interference of erstwhile pre mixed inhibitor. The micro/nano reservoir / self healing materials incorporated in the conventional coating can sense surrounding environmental changes such as pH[1,2], temperature[3], light[4,5], aggressive ionic concentration[6], mechanical action[7], electric field[8], humidity[9], pressure[10], ensures the timely release of corrosion inhibitors or healing materials to compensate defects area, providing both the excellent physical barrier effect and self-healing functionality. This development utilizes high end synthetic chemistry for the design of reservoirs and also for the release kinetics associated therein [11-24]. Porous materials with well-defined size, shape and geometry in the nano to micro-scale have fascinated research interest with greater impact in applications. These materials possess unique properties that with fibrous surface morphology, good thermal and hydrothermal stability, and high mechanical stability enable a larger increase in the surface area and access by guest species to the internal pore. Stober method is a facile and effective approach for the synthesis of mesoporous silica nanoparticles in an aqueous ethanol solution [25-29]. Template aided synthesis has been a focus of material science as it provides a unique way to prepare a variety of ordered mesostructured material with high surface areas and large, uniform pores [30-32]. However, it is difficult to obtain materials with desired pore sizes and shape because of the structural freedom of longer hydrophobic chains of surfactants normally used as templates. Aqueous cetyltrimethyl ammonium bromide (CTAB) with relatively long alkyl chain (n = 16) gives a spherical-like micelle, at wider mixing composition and allows precise control of pore geometry and pore size. Poly aspartic acid salts is a kind of biodegradable, innocuous and environmental friendly bio organic polymer, recognized as green material, and widely applied in such areas as agriculture, medicine, commodity, water treatment, petroleum, etc. [33-36]. Pioneering work by Shchukin et al. [37-40] utilizes the polyelectrolyte layer-by-layer assembly to build pH sensitive shells of nano-containers to control the release of encapsulated corrosion inhibitors and achieve a significant progress in feedback anticorrosion coatings. In this paper, the modified stober method using CTAB as template has been attempted to synthesize spherical mesoporous SiO_2 to be used as reservoir. The reservoir was loaded with poly aspartic acid (PAA) with subsequent multilayer coverage of polyelectrolytes and used as active corrosion protection coatings. More insight into the smartness of the coating established for the first time using LEIS studies.

Experimental

Synthesis of mesoporous SiO_2 (m-SiO_2)

In a typical preparation, 3 g CTAB was first dissolved in 100 mL of distilled water which is called as micelle solution. 8.5 mL of TEOS, 24 mL of ethanol and 10 mL of distilled water were added to form silanol mixture. Micelle and silanol solutions were mixed suddenly followed by the drop wise addition of 5 mL (2M) NH_4OH with continuous stirring for 15 minutes. This solution was further transferred into autoclave maintained at 120°C for 3 h. Silica which got precipitated was separated by centrifugation and dried at room temperature. The surfactant was removed by calcination at 550 °C for 5 h. The mechanism of formation of the m-SiO_2 spheres is described as follows (Fig.1a).

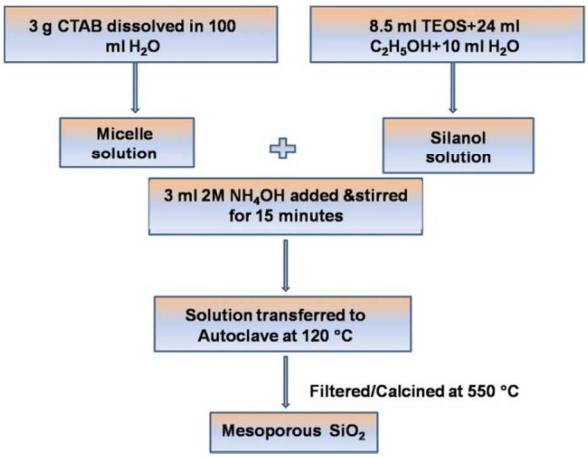

Fig.1a. Synthesis of mesoporous SiO_2

First, the TEOS molecules approach the catalyst in the aqueous phase, followed by hydrolysis of TEOS. The hydrolyzed TEOS molecules will condense at the aqueous/oil interface. Finally, the resultant negatively charged silicates and the cationic surfactant CTAB steadily self-assemble at the aqueous/oil interface to form a silica sphere.

Synthesis of Silica reservoir (SiO_2-r)

The as-synthesized silica water suspension (5 mg^3mL^{-1}) was mixed with aqueous 3M solution of poly aspartic acid (PAA, MW~155.01, 5 mg^3mL^{-1}) in a volume ratio 1:1 and stirred for 2 h.

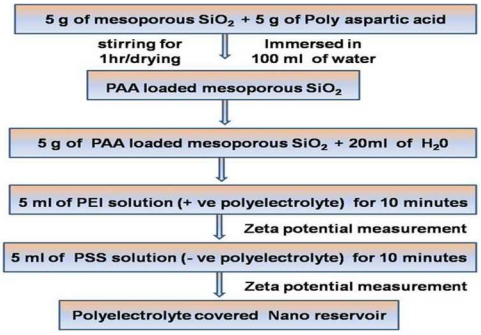

Fig.1b. Inhibitor loading and polyelectrolyte covering of SiO_2.

The loaded reservoir were separated by centrifugation and dried over night. Reservoir coverage by the PEI/PSS complex shell was done by LBL technique in three subsequent steps as reported by Shchukin (Fig.1b). In the first stage, deposition of the positively charged PEI on the negatively charged SiO_2 nanoparticles was performed by mixing 20 mL of 5 wt % SiO_2 suspensions with 5 mL of 2 mg mL^{-1} PEI solution for 10 min with constant stirring. The SiO_2/PEI sample was thus obtained washed three times by Milli-Q water. This washing procedure was performed after each deposition step. Deposition of the negative PSS layer was carried out from 5 mg mL-1 PSS solution. The resulting (Fig.1c) nano reservoir has a SiO_2 (PAA)/PEI/PSS structure.

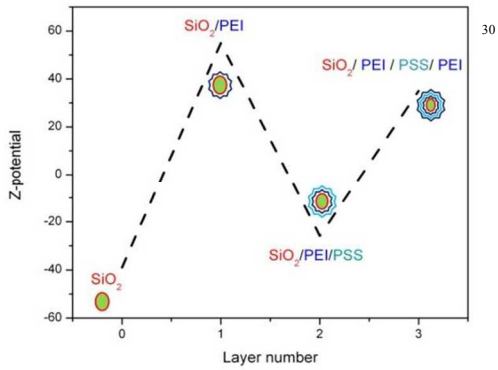

Fig.1c.Zeta potential measurements of SiO_2-r

Characterization of mesoporous SiO_2

The FTIR spectra of mesoporous of SiO_2 was recorded using Nicolet 380 (Thermo, USA) FTIR instrument having ATR attachment. The insitu FTIR was measured using FTIR microscope (Nicolet Centraurus). The morphology of the reservoir was analysed using Tescan (model vega3 SB-Easyprobe) Scanning Electron Microscope, ZEISS (model Supra-VP55) Field Emission Scanning Electron Microscope (FESEM) and Transmission electron microscopy (Tecnai - 20 (G2) (TEM). Zeta potential measurements were performed in Zetasizer (MALVERAN Nano Series, Malvern Instruments Ltd, Enigma Business Park, Grovewood Road, Malvern, Worcestershire, UK. WR14 1XZ).

The X-ray diffraction pattern was taken with PAN Analytical (Model PW 3040/60) X-ray diffractometer using Cu Kα radiation in the 2θ range of 0-90°and 0-5° at the scan rate of 0.017°/ 2θ.

Corrosion protection evaluation of with /without reservoir coated on steel.

EIS method

Power suite software was used for data acquisition of impedance using PARSTAT 2273 electrochemical workstation with an AC signals of 20 mV amplitude for a range of frequencies from 10 kHz to 0.1 Hz were impressed sequentially to the coated steel at open circuit potential. From the Bode plots the solution resistance (R_S), Coating Resistance (R_C), charge transfer resistance (R_{ct}), the double layer capacitance (C_{dl}) and coating capacitance (C_c) values were calculated by fitting the data in the equivalent circuits Fig. 2(a) and (b) using Zsimpwin software. The impedance data were analysed by using simple Randles circuit(Fig. 2(a)) for the case of uncoated steel and the circuit as shown in Fig. 2(b) for the coated steel.

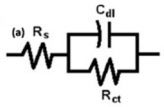

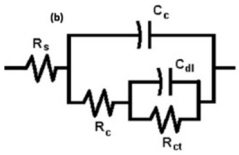

Fig. 2a.Equivalent circuit for uncoated specimen

Fig. 2b.Equivalent circuit for coated specimen

From the measured charge transfer resistance value the protection efficiency (PE) of the coatings has been obtained from the relationship.

$$\text{Protection Efficiency} = \frac{R_{ct}^{*} - R_{ct}}{R_{ct}^{*}} \times 100$$

Where R_{ct}* and R_{ct} are the charge transfer resistance values in the presence and absence of coating.

LEIS method

The LEIS measurements were performed on coated steel electrode with an artificial defect using SCV Model 470 Scanning Electrochemical Workstation, which was comprised of a 470 scanning control unit, a 3300 potentiostat, a lock in amplifier and a video camera system. The relative location of the microprobe to WE was monitored by a video camera system. The scanning micro probe was operated in two modes. LEIS was operated in two different modes. The first mode was used for the complete spectrum of LEIS measurements. The microprobe with a 10 µm tip was set directly above the defect to measure the typical impedance response at the individual point. The distance between the probe tip and the WE surface was 100µm, which was adjusted and monitored through a video camera. During LEIS measurements, an AC disturbance signal of 10mV was applied to the electrode at open circuit potential. The measuring frequency ranged from 1 MHz to 1 µHz. The second mode was used for LEIS area mapping. The microprobe was stepped over a designated area of the electrode surface. The scanning took the form of a raster in x–y plane. The step size was controlled to obtain a plot of 31 points × 31 points. The ac disturbance signal was 10mV, and the excitation frequency for impedance measurements was fixed at 50 Hz.

Active corrosion protection property evaluation

The Scanning vibrating electrode technique (SVET) instrumentation used in these experiments was from Princeton Applied Research (SCV 370 control unit). Samples prepared for SVET measurement were of 1x1 cm squares with scan area of 4000 × 4000 µm and 64 x 48 points X and Y axis. The coated sample was scribed to introduce an artificial defect of size ranging from 0.1 to 0.3 mm^2. The sample was mounted in a teflon holder and the 1% NaCl solution was added. Scans were initiated within 5 min of immersion and the data were collected for various durations. Each scan consists of 400 data points on a 20 x 20 grid, with an integration time 1s per point. A complete scan required 10 min, followed by a 5 min rest period prior to the next scan. The current density maps were plotted in 3D format over the scan area, with positive and negative current densities representing anodic and cathodic regions, respectively. The measurements were taken at the open-circuit potential.

Results and Discussion

Scanning electron microscopy (SEM) images (Figure 3a and Figure S1) show spherical SiO_2 particles with a narrow distributed size of around 100 nm in diameter. The surface of SiO_2 was roughened due to removal of surfactant upon calcination (Figure 3b). TEM images (Fig. 3c-h) indicate the formation of well-defined mesoporous structure. Nitrogen adsorption/desorption isotherm of as-prepared SiO_2 is shown in Figure 4a. The sample exhibit type I isotherm and clearly indicating the microporous nature. The narrow/low hysteresis appears at desorption section, indicating the occurrence of capillary condensation in mesopores. The Nitrogen sorption results for SiO_2 spheres calcined at 550◦C show the average pore size of 3.1 nm (BJH pore size distributions are given in Figure S2), BET surface area 458 m^2/g; the total pore volume of mesoporous silica is 0.363 cm^3/g. The analysis of poly aspartic acid loaded m-SiO_2 was estimated by Nitrogen adsorption/desorption isotherm results indicates the average pore size of 1.9 nm, BET surface area 8.3 m^2/g; the total pore volume of poly aspartic acid in m-silica is 0.181 cm^3/g. The long range ordering of as-prepared SiO_2 was investigated by XRD. The sample shows a typical broad peak at 2θ=21º corresponding to the amorphous silica (inset of Figure 4b). The broad peak may be due to small size and incomplete inner structure of the particles. Figure 4b show the low angle XRD pattern of SiO_2. Three Bragg diffraction peaks could be observed at 2θ low angles of 0.5, 2.6 and 3.4 respectively in the range of 0 to 5, which could be assigned to the (100) (110) and (200) reflections of a hexagonal symmetry structure, respectively. No other impurity peaks are present indicating the purity of the silica nanoparticles. The FTIR data (Figure S3) of SiO_2 confirms the removal of CTAB upon calcination.

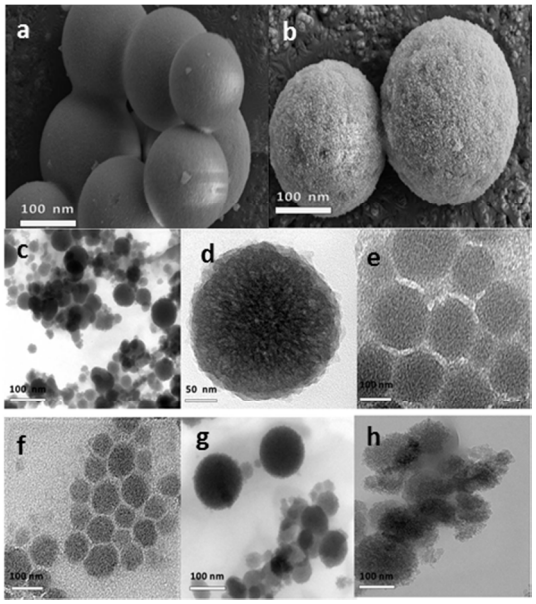

Figure 3. SEM and TEM images of mesoporous SiO_2 Caption (a)-(f) indicates different magnification of mesoporous silica.

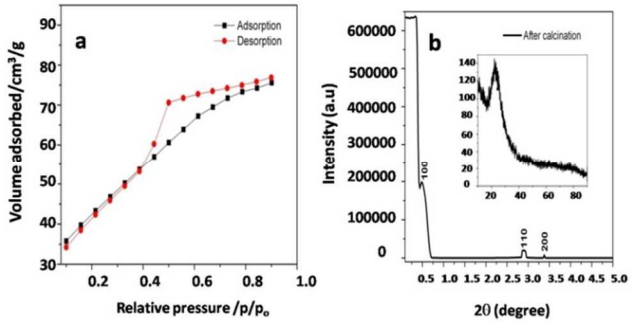

Fig.4 (a) N_2 adsorption/desorption isotherm and XRD (b) pattern of mesoporous SiO_2.

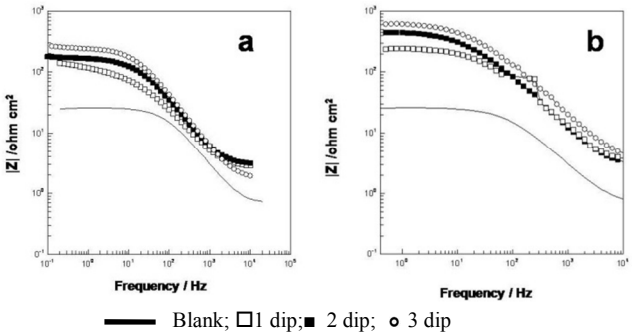

Fig.5 (a,b) EIS plot of without/with SiO_2-r coating.

Sol gel solution preparation

The organosiloxane sol was prepared by hydrolyzing (3-glycidyloxypropyl) trimethoxysilane (GPTMS) in propane-2-ol by the addition of acidified water in a molar ratio (GPTMS/propan-2-ol/ water) of 1:3:2. The final sol-gel was stirred under ultrasonic agitation for 60 min and then aged overnight at room temperature.

Evaluation of corrosion protection ability of the coating

EIS analysis

The sol-gel system was homogeneous and transparent in nature. Before coating, the metal substrates were pre-treated in pickling solution. The pre-treated substrates were coated with sol-gel and sol-gel with silica reservoir (SiO_2-r). The sol-gel films were produced by a dip-coating method. After coating, the samples were cured at 110 °C for 24 h. The corrosion behavior of without / with SiO_2-r incorporated sol gel coated steel in 1% NaCl was evaluated by EIS method. Fig.5a,b shows the Bode plot of impedance behavior of without / with SiO_2-r incorporated sol gel coated steel(Active corrosion protection coating). The impedance parameters such as coating resistance (R_c), coating capacitance (C_c), charge transfer resistance (R_{ct}), and double layer capacitance (C_{dl}) derived from these curves are given in Table 1. It can be clearly seen from the figure 5a and Table.1 that the increase in number of dipping of sol gel coating on steel surface increases the protection efficiency. The charge transfer resistance is increased from 25 Ω cm^2 corresponding to bare steel surface to 142 Ω cm^2 after 3 dipping resulting in 82% of protection efficiency. The Impedance behavior of SiO_2-r incorporated sol gel coated steel in 1% NaCl is shown in Fig. 5b. In this case, the R_{ct} value is increased drastically to 130 Ω cm^2 for the SiO_2-r incorporated coating in single dip thus offering 82% protection efficiency and with further increasing the dipping the R_{ct} values increases

No. Dipping	EIS-Sol-gel coating					EIS- Active corrosion protection coating				
	R_c Ω cm^2	C_c F/cm^2	R_{ct} Ω cm^2	C_{dl} F/cm^2	P.E %	R_c Ω cm^2	C_c F/cm^2	R_{ct} Ω cm^2	C_{dl} F/cm^2	P.E %
Blank	–	–	25	7.4×10^{-5}	–	–	–	25	7.4×10^{-5}	–
1	37	3.4×10^{-3}	101	9.4×10^{-5}	75	112	1.1×10^{-5}	130	7.0×10^{-5}	80
2	59	3.3×10^{-3}	110	6.7×10^{-5}	77	133	1.3×10^{-5}	291	2.7×10^{-5}	91
3	72	2.7×10^{-5}	142	3.7×10^{-5}	82	159	7.6×10^{-5}	408	9.4×10^{-6}	93

Table 1 EIS analysis of sol gel and active corrosion protection coating on mild steel in 1% NaCl.

marginally and showed 92% protection efficiency after 3 dipping. Besides, the coating capacitance values of SiO_2-r coated steel are found to be very less indicating the compact nature of the coating. On comparing the coating resistance values, the coating resistance for reservoir incorporated coated steel is 159 Ω cm^2 which is one times higher than that of sol gel coated steel. The higher coating resistance values in the case of reservoir incorporated coated steel indicates the formation of more compact coating. These results show that reservoir incorporated have improved the protective nature of coating.

LEIS analysis

Fig. 6a shows the Bode diagrams of pure sol gel coating was measured directly above the defect area at the various immersion times, i.e., 0, 30, 60 and 1200 minutes, respectively. It was seen that, after initial immersion, LEIS plot exhibited the impedance magnitude at low frequency decreased remarkably from 30 to 60 minutes of immersion, and then decreased continuously with the immersion time. The low frequency impedance at 0.01 Hz was approximately 2.87×10^2Ω cm^2, which was lower than that measured at defect area in initial immersion(4.61×10^2Ω cm^2) (Fig. 6a).Fig. 6b shows Bode diagrams of SiO_2-r incorporated sol gel coating was measured directly above the defect area at different immersion times such as 0, 30 60 and 1200 minutes respectively. It was seen that the impedance magnitude at low frequency increased remarkably from 30 to 60 minutes of immersion, and then increased continuously with the immersion time (ie. 1200 minutes).The low frequency impedance at 0.01 Hz was approximately 1.15×10^3Ω cm^2, which was higher than that measured at defect area in initial immersion (3.61×10^2Ω cm^2) (Fig. 6b).

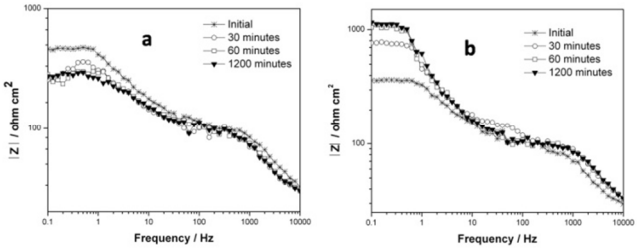

(a) Without reservoir; (b) With reservoir

Fig.6 (a,b) LEIS plot of without/with SiO_2-r coating.

Figures 7a-d shows the maps of localized impedance over the specimen from 0 to 1200 minutes of exposure in 1% NaCl. The defect area in the coating corresponds identically to the lowest value of impedance map. Obviously, the mapping technique demonstrates the lowest resistance in the artificial defect surface. After initial immersion such as 30 minutes, the defect area on the impedance map (Fig. 7b), and this is reflected the large decrease in localized impedance at the defect.

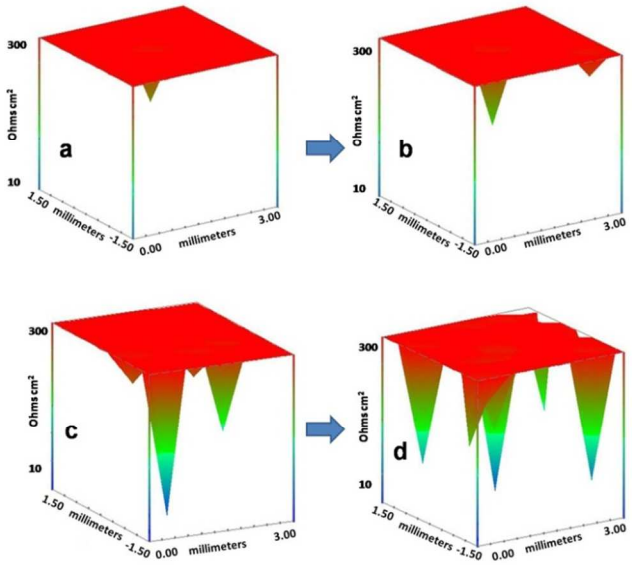

Fig.7 (a-d) LEIS area plot of pure sol gel coating.

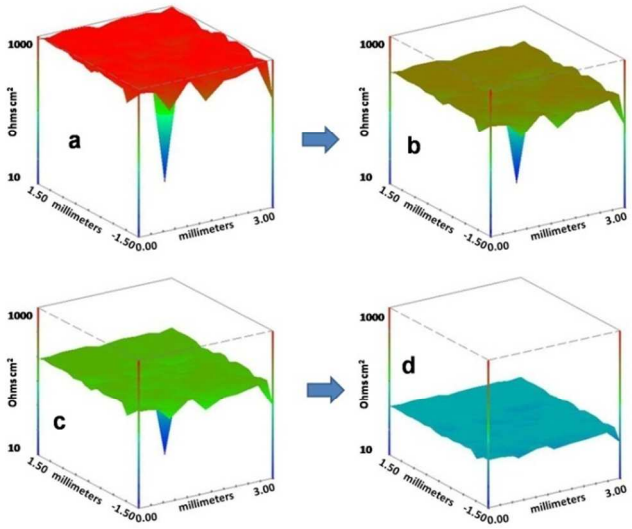

Fig.8 (a-d) LEIS area plot of active corrosion protection coating.

After 60 minutes, significant under film corrosion has increased (Fig.7c). After 1200 minutes of immersion, the original area of under film corrosion has further increased (Fig.7d) and this coincides with a substantial decrease in localized impedance at the defect and visible in the area map. Figures 8a-d shows the maps of localized impedance over the SiO_2-r incorporated sol gel coating specimen exposure in 1% NaCl with 0 to 1200 minutes respectively. Initially active corrosion protection coating on defect area has low value of impendence map. After 30 minutes, the impedance map of SiO_2-r incorporated sol gel coating (Fig. 8b) increased at the defect area. Further 60 minutes of immersion impedance value further increased (Fig. 8c). Finally, 1200 minutes of immersion, the defect area completely passivated by Poly aspartic acid. Further, increase in localized impedance value at the defect area map (Fig. 8d).

Insitu FTIR analysis

The IR spectra from down to up are corresponding to the two samples are described in Fig.9 (a,b).

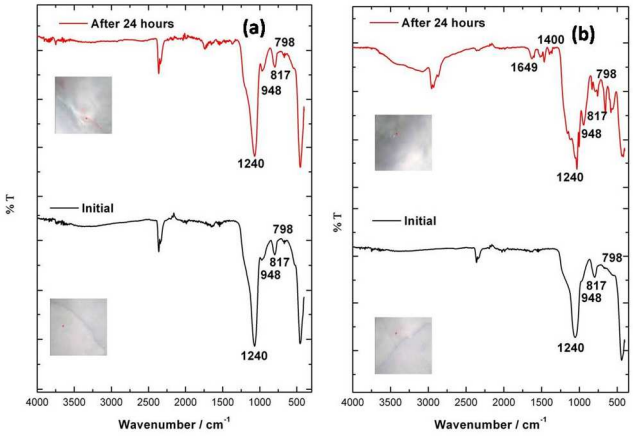

Fig.9.(a,b) FTIR analysis of local spot without/with reservoir coating.

A broad intense peak at 1240 cm^{-1}, due to the symmetrical stretching or ring breathing frequency of the epoxide ring, confirms the presence of Si-O-Si bridging sequences. The peak at 948 cm^{-1} is due to the residual organic group and results in asymmetric vibration of Si-OH bonding. The vibration of Si-O occurs at 798 cm^{-1}. The band at 817 cm^{-1} confirms the symmetric stretching vibrations of Si-O-Si bonds belonging to ring structure. The peaks at 1649 and 1400 cm^{-1} is due to the presence of stretching vibration of amide group and free carboxylic acid in poly aspartic acid.

Active corrosion protection analysis

SVET technique was used to study the active corrosion protection of without / with SiO_2-r incorporated sol gel coating on steel surface in 1% NaCl, for different durations of exposure Fig.10a depicts the local current maps over the surface of pure sol gel coated mild steel recorded immediately after exposure to 1% NaCl (i.e. after 5 min). A steep anodic current flow in the flaw area indicates the occurrence of accelerated corrosion. With continued exposure, the corrosion activity at the defect areas spreads laterally as evidenced by the increase in width of the current flow pattern in 30 minutes exposure (Fig 10a). Fig.10b shows the SVET current mapping for SiO_2-r incorporated sol gel coating on mild steel. As shown, there is an anodic current flow at the defect area at the initial instant. Fig.10b shows the current density map for coated steel after 30 minutes immersion in 1% NaCl. The anodic current flow area decreases dramatically at the defect area. We observed that the anodic current flow at the defect area gets suppressed and maintained at very low current flow. Visually it has been observed that the defect is covered with a dark passive film. This clearly demonstrates the smart property

of SiO_2-r incorporated sol gel coating over steel surface.

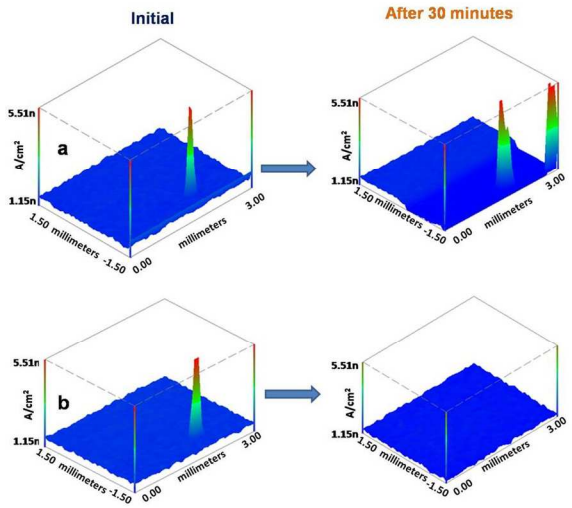

Fig.10.(a) SVET plot of pure sol gel coating

(b) SVET plot of active corrosion protection coating

In the case of the sample with a coating containing SiO_2-r, the corrosion protection is triggered by the corrosion process itself. It is well known that the corrosion process is accomplished by cathodic oxygen reduction resulting in the formation of OH- ions. This accumulated OH- ions increases the local pH which causes morphological deformations of polyelectrolyte layers and hence the inhibitor is released from the SiO_2-r network in a sufficient amount, without undesired leakage, to stop the corrosion. The anticorrosive effect of the organic inhibitor poly aspartic acid (PAA) is based on forming a film on the metal surface acting as a physical barrier for the aggressive medium [41-48].

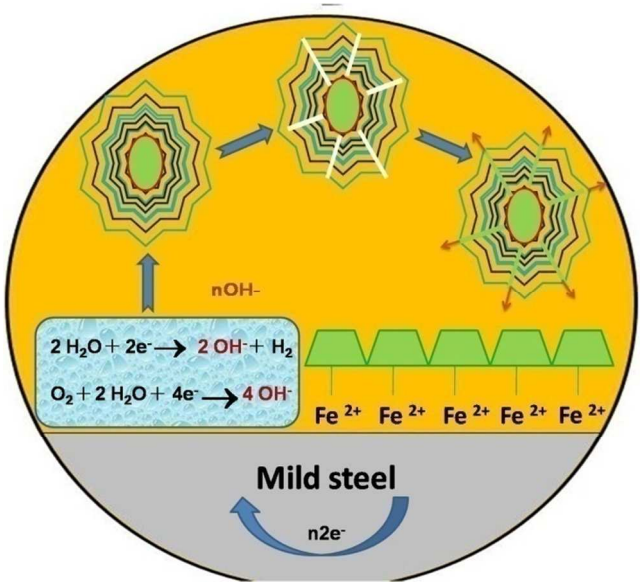

Fig.11. Mechanism of active corrosion protection coating.

Based on these observations, a suitable mechanism has been proposed as presented in Fig.11 which is self-explanatory. In summary, a new route, slightly improved version, combining the micro emulsion followed by hydrothermal process has been attempted for preparing m-SiO_2 spheres. CTAB is used as the surfactant and the silica shells were self-assembled at the interface via ammonia catalyzed hydrolysis and condensation of TEOS. The excess amount of organic components was removed from the m-SiO_2 spheres by the treatment with distilled water, in which the mesoporous spheres could maintain the complete spherical structure. Prepared spheres were porous and abundance of pores with average pore size of 3.1 nm was formed in the shell. The smartness of the coating containing inhibitor loaded mesoporous silica reservoir was evaluated by spot and area mapping LEIS which is supported by SVET studies.

Conclusions

Modified synthetic strategy will become a general method to systematically manipulate the expected shapes and sizes of inorganic compounds at the nanoscale range. The corrosion efficiency of a new active coating system consisting of a sol-gel coating with and without PAA loaded mesoporous silica nano reservoir has been evaluated. Furthermore, well-pronounced active corrosion protection properties were confirmed by EIS, LEIS and LEIS mapping, FTIR and SVET measurements.

Acknowledgements

The authors wish to express their sincere thanks to the Director, CECRI, Karaikudi for his encouragement. The authors thank CSIR, New Delhi for financial support through the 12th Five Year Plan network project IntelCOAT (CSC0114).

Notes and references

[a]*Corrosion and materials protection division, CSIR-Central Electrochemical Research Institute, Karaikudi-630006, India. sathya_cecri@yahoo.co.in; sathya@cecri.res.in*

† Electronic Supplementary Information (ESI) available: [SEM, FTIR data of porous silica]. See DOI: 10.1039/b000000x/

[1]M. A. Jakab, J. R. Scully, *Nat. Mater.,* 2005, **4**, 667.
[2]E. V. Skorb, D. Fix, D. V. Andreeva, H. Mohwald, D. G. Shchukin, *Adv. Funct. Mater.,* 2009, **19**, 2373.
[3]G. L. Li, Z. L. Zheng, H. Mohwald, D. G. Shchukin, *ACS Nano* 2013, **7**, 2470.
[4]E. V. Skorb, A. G. Skirtach, D. V. Sviridoc, D. G. Shchukin, H. Mohwald, *ACS Nano* 2009, **3**, 1753.
[5]E. V. Skorb, D. V. Sviridov, H. Mohwald, D. G. Shchukin, *Chem. Commun.*, 2009, **40**, 6041.
[6]J. Tedim, M.L. Zheludkevich, A.N. Salak, A. Lisenkov, M.G.S. Ferreira, *J. Mater. Chem.,* 2011, **21**, 15464.
[7]S. H. Hu, C. H. Tsai, C. F. Liao, D. M. Liu, S. Y. Chen, *Langmuir* 2008, **24**, 11811.
[8]D. G. Shchukin, D. O. Grigoriev, H. Mohwald, *Soft Matter* 2010, **6**, 720.
[9]Y. Dou, A. Zhou, T. Pan, J. Han, M. Wei, D. G. Evans, X. Duan, *Chem. Commun.,* 2014, **50**, 7136.
[10]C. Hou, T. Huang, H. Wang, H. Yu, Q. Zhang, Y. Li, *Sci.Rep.,* 2013, **3**, 03138-1.
[11]A.S. Hamdy, I. Doench, H. Möhwald, *Pro. Org. Coat.,* 2011, **72**, 387.
[12] M. Saremi , M. Yeganeh,*Corros. Sci.,* 2014, **86**, 159.
[13] I.A. Kartsonakis, A.C. Balaskas, E.P. Koumoulos, C.A. Charitidis, G. Kordas, *Corros. Sci.,* 2012,**65**, 481.
[14] W. Wang, L. Xu, X. Li, Y. Yang, E. An, *Corros. Sci.,* 2014 ,**80**, 528.
[15] I.A. Kartsonakis, E.P. Koumoulos, A.C. Balaskas, G.S. Pappas, C.A. Charitidis, G.C. Kordas, *Corros. Sci.,* 2012, **57**, 56.
[16] I.A. Kartsonakis, A.C. Balaskas, G.C. Kordas, *Corros. Sci.,* 2011, **53**, 3771.
[17] A. Ait Aghzzaf, B. Rhouta, E. Rocca, A. Khalil, J. Steinmetz, *Corros. Sci.,* 2014, **80,** 46.

[18] G. Williams, S. Geary, H.N. McMurray, *Corros. Sci.,* 2012, **57**, 139.
[19] M.L. Zheludkevich, S.K. Poznyak, L.M. Rodrigues, D. Raps, T. Hack, L.F. Dick, T. Nunes, M.G.S. Ferreira, *Corros. Sci.,* 2010, **52**, 602.
[20] J.-H. Syu, J.-Y. Uan, M.-C. Lin, Z.-Y. Lin, *Corros. Sci.,* 2013, **68**, 238.
[21] D.G. Shchukin, M. Zheludkevich, K. Yasakau, S. Lamaka, M.G.S. Ferreira, H. Mohwald, *Adv. Mater.,* 2006, **18**, 1672.
[22] D.V. Andreeva, E.V. Skorb, D.G. Shchukin, *ACS Appl. Mater. Inter.,*2010, **2**, 1954.
[23] S.A.S. Dias, S.V. Lamaka, C.A. Nogueira, T.C. Diamantino, M.G.S. Ferreira, *Corros. Sci.,* 2012, **62**, 153.
[24] D. Song, X. Jing, J. Wang, Y. Wang, P. Yang, M. Zhao, M. Zhang, *Corros. Sci.,* 2011, **53**, 1732.
[25] D. Borisova, H. Mohwald, D.G. Shchukin, *ACS Nano* 2011, **5**, 1939.
[26] M.G. Run, I. Lauer, K.K. Unger,*Adv. Mater.,* 1997, **9**, 254.
[27] L. Xu, J. He, *J. Mater. Chem.C*., 2013, **1**,4655.
[28] Q. Hulo, D.I. Margolese, G.D. stucky, *Chem. Mater.,* 1996, **8**, 1147.
[29] G. L.Li, M. Schenderlein, Y. Men, H. Möhwald, D.G. Shchukin, *Adv. Mater. Inter.,* 2013, **1**, 1C.
[30] C. T. Kresge, M. E. Leonowicz, W. J. Roth, J.C. Vartuli, J. S. Beck, *Nature* 1992, **359**, 710.
[31]J.S.Beck, J.C. Vartuli, W.J.Roth, M.E. Leonowicz, C.T.Kresge,K.D.Schmitt, C.T.W. Chu, D.H. Oslan, E.W. Sheppard, S.B.MaCullen, J.B. Higgins, J.L. Schlenker, *J. Am. Chem. Soc.,* 1992, **114**, 10834.
[32] Z. Teng, G. Zeng, Y. Dou, W. Li, C.Y. Mou, X. Zhang, A.M.Asiri, D. Zhao,*Angew. Chem. Int. Ed.*, 2012, **51**, 2173.
[33] K. Kataoka, *Pure Appl. Chem. A*., 1994, **31**, 759.
[34] T. Ehtezazi, T. Govender, S. Stolnik*, Pharm. Res.*, 2000, **17**, 871.
[35] P. Guenoun, H.T. Davis, M. Tirrell, J.W. Mays, *Macromolecules* 1996, **29**, 3965.
[36] H.L. Jiang, K.J. Zhu, *J. Appl. Polym. Sci.,* 2006, **9**, 2320.
[37] M.L. Zheludkevich, D.G. Shchukin, K.A. Yasakau, H. Mohwald, M.G.S. Ferreira, *Chem. Mater.,* 2007, **19**, 402.
[38]D.G Shchukin, H. Mohwald, Adv. Funct. Mater., 2007, 17, 1451.
[39]D.V. Andreeva, E.V. Skorb, D.G. Shchukin, *ACS Appl. Mater. Inter.,* 2010, **2**, 1954.
[40]D.O. Grigoriev, K. Kohler, E. Skorb, D. G. Shchukin, H. Mohwald, *Soft Matter* 2009, **5**, 1426.
[41]C.H. Hsu, F. Mansfield, Corrosion 2001, **57**, 747.
[42] J. He, V. Johnston Gelling, D.E. Tallman, G.P. Bierwagen, *J. Electrochem. Soc.,* 2000, **147**, 3661.
[44] C. Scheffey, *Rev. Sci. Instru.,* 1988, **59**, 787.
[45] J. Fu T. Chen, M.D. Wang, N.W. Yang, S.N. Li, Y. Wang, X. D.Liu**,** *ACS Nano* 2013, **7**, 11397.
[46] D. Kowalski, M. Ueda, T. Ohtsuka, *J. Mater. Chem.,* 2010, **20**, 7630.
[47] A. Yabuki, K. Okumura, *Corros. Sci.,* 2012,**59**, 258.
[48] I.A. Kartsonakis, A.C. Balaskas, E.P. Koumoulos, C.A. Charitidis, G.C. Kordas, *Corros. Sci.,* 2012, **57**, 30.